

# Ultrafast energy absorption and photoexcitation of bulk plasmon in crystalline silicon subjected to intense ultrashort laser pulses

Tzveta Apostolova,<sup>1,2</sup> Boyan Obreshkov,<sup>1</sup> and Iaroslav Gnilitskyi<sup>3,4,5</sup>

<sup>1</sup>*Institute for Nuclear Research and Nuclear Energy,  
Bulgarian Academy of Sciences, Tsarigradsko chausse 72, 1784 Sofia, Bulgaria*

<sup>2</sup>*Institute for Advanced Physical Studies,  
New Bulgarian University, 1618 Sofia, Bulgaria*

<sup>3</sup>*NoviNano Lab LLC, Pasternaka 5, 79015 Lviv, Ukraine*

<sup>4</sup>*Department of Photonics, Lviv Polytechnic National University,  
Stepana Bandery 14, 79000, Lviv, Ukraine*

<sup>5</sup>*University of Modena and Reggio Emilia (UNIMORE),  
Amendola 2, 42122 Reggio Emilia, Italy*

## Abstract

We investigate the non-linear response and energy absorption in bulk silicon irradiated by intense 12fs near-infrared laser pulses. Depending on the laser intensity, we distinguish two regimes of non-linear absorption of the laser energy: for low intensities, energy deposition and photoionization involve perturbative three-photon transition through the direct bandgap of silicon. For laser intensities near and above  $10^{14}$  W/cm<sup>2</sup>, corresponding to photocarrier density of order  $10^{22}$  cm<sup>-3</sup>, we find that absorption at near-infrared wavelengths is greatly enhanced due to excitation of bulk plasmon resonance. In this regime, the energy deposited onto electrons exceeds a few times the thermal melting threshold of Si. The optical reflectivity of the photoexcited solid is found in good qualitative agreement with existing experimental data. In particular, the model predicts that the main features of the reflectivity curve of photoexcited Si as a function of the laser fluence, are due to state and band filling effects associated with Pauli blocking rather than Drude free-electron response. The non-linear response of the photoexcited solid is investigated for irradiation with a sequence of two strong and temporary non-overlapping pulses. We find that the cumulative effect of the two pulses is non-additive in terms of deposited energy. More specifically, and depending sensitively on the pump laser intensity, photoionization and energy absorption on the rising edge of the second pulse is enhanced due to superposition of the electric fields of bulk plasmon and the laser. When increasing the intensity above this threshold, the electric field of the second pulse is screened out and most of its energy is reflected away.

## I. INTRODUCTION

Time-resolved optical experiments on femtosecond laser excited dielectrics<sup>1–11</sup> provide evidence that ultrafast solid to liquid phase transition occurs after a large amount of laser energy is deposited in the solid material during a time interval much shorter than the thermalization of the absorbed energy. The photoexcitation of a critical number of electron-hole pairs results in bond softening and structural phase transition. Theoretical models<sup>12–15</sup> were developed aiming to investigate electronically-driven ultrafast melting mechanism in semiconductors. These studies predict that lattice instability in the dense plasma develops once the critical density of electron-hole pairs is of order  $10^{22} \text{ cm}^{-3}$ . For instance in silicon irradiated with visible wavelengths, such high densities are reached at the fluence of about  $0.2 \text{ J/cm}^2$ <sup>16</sup>.

The high density plasma of photoexcited charge carriers leads to distinct change of the optical reflectivity. Changes of optical constants of the strongly excited dielectrics are measured using pump-probe spectroscopy techniques<sup>4,16–18</sup>. The optical reflectivity of photoexcited silicon as a function of the pump pulse fluence was measured in Ref.<sup>16</sup> for the 625 nm wavelength. At very early times (150 fs after the excitation), when the plasma is not yet thermalized, the experimental data showed that the reflectivity initially decreases for relatively low pump fluences until it reaches a minimum at  $0.2 \text{ J/cm}^2$ . By increasing the pump fluence above that value, a sharp rise of reflectivity of the probe pulse was observed. The fluence dependence of the reflectivity curve was consistently interpreted within a simplified Drude model for the dielectric function of the optically excited Si, i.e. assuming that the optical properties are dominated by free-carrier response.

Dielectric properties of photoexcited solids are often modeled with Drude response of free carriers embedded in a dielectric medium<sup>19,20</sup>. More elaborate model for the macroscopic dielectric function of the laser-excited state incorporating Pauli blocking and screening of the Coulombic electron-hole attraction was proposed in Ref.<sup>21,22</sup>. Good qualitative agreement with measured dielectric function of gallium arsenide was found<sup>6</sup>. More recently, first principle approaches based on time-dependent density functional theory (TDDFT) have been developed and applied for understanding the optical properties of strongly excited semiconductors and dielectrics. Ultrafast optical breakdown thresholds of dielectrics such as diamond and silica were obtained using TDDFT<sup>23,24</sup>. With the increase of the light

pulse intensity, the number of photoexcited charge carriers increases and dense plasma of electron-hole pairs is established. When the corresponding plasma frequency matches the laser frequencies, a resonant energy transfer occurs from the light pulse to the electrons and dielectric breakdown occurs associated with sharp rise of the optical reflectivity. In Ref.<sup>25</sup>, the reflectivity of photoexcited silicon was calculated as a function of the peak laser intensity and a qualitative agreement with the experimental observation in Ref.<sup>16</sup> was found. Consistent interpretation of the intensity dependence of the reflectivity curve was given in terms of simplified free electron Drude model. In Ref.<sup>26,27</sup>, the dielectric response of the crystalline silicon following irradiation by a high intensity near-infrared laser pulse was obtained from numerical pump-probe experiments. The results showed that the excited silicon exhibits characteristic features of electron-hole plasma in nonequilibrium phase. The real part of the dielectric function was found to be well described by a Drude free-carrier response with screened plasma frequency determined from ground state properties. The effective mass of the charge carriers was found to increase monotonically with the increase of the laser intensity. Optical anisotropy in the response of the photoexcited solid was also reported.

While standard pump-probe spectroscopy studies electronic dynamics with femtosecond time resolution, advances in laser technologies resulted in the attosecond metrology<sup>28,29</sup>. In nonlinear attosecond polarization spectroscopy<sup>30</sup>, the oscillating laser electric field is used to measure the non-linear polarization which in turn determines the amount of energy reversibly or irreversibly exchanged between the electromagnetic field and the dielectric material. Nonlinear polarization spectroscopy yields more complete information about the dynamic electronic response to strong fields with attosecond time resolution. For instance, measurements utilizing attosecond spectroscopy in combination with TDDFT calculations allowed to resolve electron dynamics in crystalline silicon<sup>31</sup>. Interest in the time evolution of the excitation process is motivated by applications like petahertz signal processing<sup>32,33</sup> and mechanisms of ultrafast dielectric breakdown<sup>34–42</sup>.

The optical breakdown thresholds are associated with femtosecond laser ablation<sup>43–46</sup>. During femtosecond laser ablation laser-induced periodic surface structures (LIPSS) form under certain irradiation conditions. Typically LIPSS occur after irradiation by multiple laser pulses. Two of the main mechanisms of LIPSS formation are interference of laser induced surface plasmon polaritons with the incident field<sup>47</sup> and hydrodynamic instability<sup>48</sup>. The plasmon mechanism of ripple formation is due to the spatial modulation of the photo-

electron density after the interference between the incident and a surface-scattered wave<sup>49</sup> intermediated by surface roughness. A grating assisted interference between the driving laser and photoinduced surface plasma oscillations was demonstrated in optical reflectivity measurements of photoexcited silicon surface<sup>50</sup>. Advances in technologies found a regime where highly regular LIPSS (HR-LIPSS) are produced - a few temporally overlapping identical femtosecond laser pulses with above threshold fluence<sup>51,52</sup>. In contrast to the standard processing procedure utilizing multiple laser pulses with near threshold fluences. Such approach allows substantially improve production rate of producing nanostructures on large surface area.

In this paper we report the time evolution of the conduction electron density and excitation of collective plasma oscillations of the electron gas in crystalline silicon irradiated by intense ultrashort near infrared laser pulse. Depending on the laser intensity, we distinguish two regimes of non-linear absorption: low-intensity regime when laser energy is transferred to electrons by three- and four-photon transitions, and high-intensity regime when energy is resonantly transferred to plasmons. Scaling laws of the absorbed energy and electron density as a function of the laser intensity are obtained. Optical constants and the reflectivity of the photo excited silicon are derived and compared to existing experimental data. The interference of the plasmons with the driving laser following the irradiation by a double pulse sequence resulting in highly efficient energy transfer is also demonstrated.

The paper is organized as follows: Sec. II includes our theoretical method based on self-consistent solution of the coupled time-dependent Schrödinger-Maxwell's equations. Sec III presents numerical results and discussion of the nonlinear response of silicon subjected to pair of intense 12fs near-infrared laser pulses. Sec IV includes our main conclusions.

## II. THEORETICAL FORMALISM

In velocity-gauge, the Schrödinger in single-active electron approximation is

$$i\partial_t|\psi_{v\mathbf{k}}(t)\rangle = H(t)|\psi_{v\mathbf{k}}(t)\rangle \quad (1)$$

here  $v\mathbf{k}$  labels the initially occupied Bloch states in the valence band with definite crystal momentum  $\mathbf{k}$ ,  $H(t)$  is the time-dependent Hamiltonian

$$H(t) = \frac{1}{2}[\mathbf{p} + \mathbf{A}(t)]^2 + V(\mathbf{r}), \quad (2)$$

In the empirical pseudopotential method<sup>53</sup>, the periodic ionic lattice potential is presented by a plane wave-expansion in the basis of reciprocal lattice wave-vectors

$$V(\mathbf{r}) = \sum_{\mathbf{G}} V(G) \cos(\mathbf{G} \cdot \boldsymbol{\tau}) e^{i\mathbf{G} \cdot \mathbf{r}} \quad (3)$$

where  $2 \boldsymbol{\tau} = a_0/4(1, 1, 1)$  is the relative vector connecting two Si atoms in a crystal unit cell and  $a_0 = 5.43 \text{ \AA}$  is the bulk lattice constant. The pseudopotential formfactors (in Rydberg) are  $V(G^2 = 3) = -0.21$ ,  $V(G^2 = 8) = 0.04$  and  $V(G^2 = 11) = 0.08$ .

The macroscopic vector potential is split into applied laser and induced vector potentials  $\mathbf{A}(t) = \mathbf{A}_{\text{ext}}(t) + \mathbf{A}_{\text{ind}}(t)$ , the total pulsed electric field is  $\mathbf{E}(t) = -d\mathbf{A}/dt$ . The applied vector potential is related to the electric field of the incident laser by  $\mathbf{E}_{\text{ext}} = -d\mathbf{A}_{\text{ext}}(t)/dt$ , which we parametrize by a temporary Gaussian function

$$\mathbf{E}_{\text{ext}}(t) = \mathbf{e} e^{-\ln(4)t^2/\tau_L^2} \cos \omega_L t \quad (4)$$

where  $\mathbf{e}$  is a unit vector in the direction of the laser polarization,  $\omega_L$  is the laser frequency corresponding to photon energy  $\hbar\omega_L$  and  $\tau_L$  is the pulse length. The vector potential  $\mathbf{A}_{\text{ind}}(t)$  is a result of the induced dipole moment per unit volume  $\mathbf{P}(t)$  inside the bulk, which we determine self-consistently by solving the Maxwell's equation

$$\frac{d^2 \mathbf{A}_{\text{ind}}(t)}{dt^2} = 4\pi \mathbf{J}(t), \quad (5)$$

here  $\mathbf{J}(t)$  is the macroscopic electric current density

$$\mathbf{J}(t) = \sum_v \int_{\text{BZ}} \frac{d^3 \mathbf{k}}{4\pi^3} \langle \psi_{v\mathbf{k}}(t) | \mathbf{v}(t) | \psi_{v\mathbf{k}}(t) \rangle \quad (6)$$

and  $\mathbf{v}(t) = \mathbf{p} + \mathbf{A}(t)$  is the velocity operator. The induced polarization is  $\mathbf{P}(t) = \int^t dt' \mathbf{J}(t')$ , the absorbed laser energy per unit volume at time  $t$  is calculated from the work done by the pulsed laser field in moving the electrons

$$\Delta E(t) = \int_{-\infty}^t dt' \mathbf{E}(t') \cdot \mathbf{J}(t') \quad (7)$$

### A. Linear response of photoexcited Si

In the remote past  $t \rightarrow -\infty$ , the laser vector potential vanishes  $\mathbf{A}_{\text{ext}} = \mathbf{0}$  and the Maxwell's equation exhibits a trivial solution with  $\mathbf{A} = \mathbf{0}$ . The electrons are in a ground

state characterized by occupation numbers of Bloch states  $f_{n\mathbf{k}}^0 = \{0, 1\}$ . However in the remote future  $t \rightarrow +\infty$ , when the applied laser vector potential has vanished  $\mathbf{A}_{\text{ext}} = \mathbf{0}$ , the Maxwell's equation may exhibit a non-trivial solution with  $\mathbf{A}(t) \neq \mathbf{0}$ . In this case, electrons are driven by the self-induced polarization. The single-particle density matrix evolves in time according to

$$i\frac{d\rho}{dt} = [H, \rho]. \quad (8)$$

where  $H = H_0 + V$ , here  $H_0$  is the field-free Hamiltonian and  $V = \mathbf{A} \cdot \mathbf{p}$  is the interaction with the self-induced gauge vector potential. Treating this interaction as weak, we split  $\rho = \rho_0 + \delta\rho$ , such that  $i d\rho_0/dt = [H_0, \rho_0]$ . Because photoionization has created electron-hole pairs in coherent superposition of states, the unperturbed density matrix is non-diagonal in a Bloch state basis and takes the form

$$[\rho_0(t)]_{nn'\mathbf{k}} = \xi_{nn'\mathbf{k}} e^{-i\omega_{nn'\mathbf{k}}t}, \quad (9)$$

where the diagonal elements  $\xi_{nn\mathbf{k}} = f_{n\mathbf{k}} = \sum_v |\langle n\mathbf{k} | \psi_{v\mathbf{k}}(\infty) \rangle|^2$  are the laser-intensity dependent occupation numbers of single particle states, the off-diagonal elements give the interband coherences and  $\omega_{nn'\mathbf{k}} = \varepsilon_{n\mathbf{k}} - \varepsilon_{n'\mathbf{k}}$  are the transition frequencies. To first order in perturbation theory, the equation of motion is

$$i\frac{d\delta\rho}{dt} = [H_0, \delta\rho] + [V, \rho_0] \quad (10)$$

which reads in components

$$i\frac{d}{dt}\delta\rho_{nn'\mathbf{k}} = \omega_{nn'\mathbf{k}}\delta\rho_{nn'\mathbf{k}}(t) + \sum_{n''} [V_{nn''\mathbf{k}}(t)\xi_{n''n'\mathbf{k}}e^{-i\omega_{n''n'\mathbf{k}}t} - \xi_{nn''\mathbf{k}}e^{-i\omega_{nn''\mathbf{k}}t}V_{n''n'\mathbf{k}}(t)] \quad (11)$$

Because interband coherences include rapidly varying phases, such terms tend to average to zero, only diagonal terms with  $n'' = n$  and  $n'' = n'$  give dominant contribution, such that the equations of motion simplify to

$$i\frac{d}{dt}\delta\rho_{nn'\mathbf{k}} \approx \omega_{nn'\mathbf{k}}\delta\rho_{nn'\mathbf{k}} + V_{nn'\mathbf{k}}(t)(f_{n'\mathbf{k}} - f_{n\mathbf{k}}) \quad (12)$$

The Fourier transformation of this result gives

$$\delta\rho_{nn'\mathbf{k}}(\omega) = \frac{V_{nn'\mathbf{k}}(\omega)(f_{n'\mathbf{k}} - f_{n\mathbf{k}})}{\omega_{n'\mathbf{k}} - \omega} \quad (13)$$

and therefore the Cartesian components of the current can be written

$$J_\alpha(\omega) = \sigma_{\alpha\beta}(\omega)E_\beta(\omega) \quad (14)$$

in terms of conductivity tensor of the photoexcited solid

$$\sigma_{\alpha\beta}(\omega) = \frac{1}{i\omega} \sum_{nn'} \int \frac{d^3\mathbf{k}}{4\pi^3} \frac{(f_{n\mathbf{k}} - f_{n'\mathbf{k}})(p_{\alpha})_{nn'\mathbf{k}}(p_{\beta})_{n'\mathbf{k}}}{\omega_{n'\mathbf{k}} - \omega} - \frac{n_0}{i\omega} \delta_{\alpha\beta}, \quad (15)$$

here  $n_0 = 32/a_0^3$  is the average bulk density. The associated linear susceptibility tensor  $\chi_{\alpha\beta}(\omega) = i\sigma_{\alpha\beta}(\omega)/\omega$  of the photoexcited solid is divergent when  $\omega \rightarrow 0$ , to display this divergence,  $\chi$  can be split into interband and intraband contributions<sup>54</sup>

$$\chi_{\alpha\beta} = \frac{1}{\omega^2} A_{\alpha\beta} + \frac{1}{\omega} B_{\alpha\beta} + C_{\alpha\beta} \quad (16)$$

where

$$C_{\alpha\beta} = \sum_{nn'} \int_{\text{BZ}} \frac{d^3\mathbf{k}}{4\pi^3} \frac{(f_{n\mathbf{k}} - f_{n'\mathbf{k}})(p_{\alpha})_{nn'\mathbf{k}}(p_{\beta})_{n'\mathbf{k}}}{\omega_{n'\mathbf{k}}^2(\omega_{n'\mathbf{k}} - \omega)} \quad (17)$$

is regular at  $\omega = 0$ , and the coefficients in front of the divergent terms are

$$B_{\alpha\beta} = \sum_{nn'} \int_{\text{BZ}} \frac{d^3\mathbf{k}}{4\pi^3} \frac{(f_{n\mathbf{k}} - f_{n'\mathbf{k}})(p_{\alpha})_{nn'\mathbf{k}}(p_{\beta})_{n'\mathbf{k}}}{\omega_{n'\mathbf{k}}^2}, \quad (18)$$

$$A_{\alpha\beta} = - \sum_n \int_{\text{BZ}} \frac{d^3\mathbf{k}}{4\pi^3} f_{n\mathbf{k}} \left( \frac{1}{m_{n\mathbf{k}}^*} \right)_{\alpha\beta}. \quad (19)$$

In Eq.(19),  $[1/m_{n\mathbf{k}}^*]_{\alpha\beta}$  are the Cartesian components of the inverse effective mass tensor of band  $n$  with crystal momentum  $\mathbf{k}$

$$\left( \frac{1}{m_{n\mathbf{k}}^*} \right)_{\alpha\beta} = \delta_{\alpha\beta} - \sum_{n' \neq n} \frac{(p_{\alpha})_{nn'\mathbf{k}}(p_{\beta})_{n'\mathbf{k}} + (p_{\beta})_{nn'\mathbf{k}}(p_{\alpha})_{n'\mathbf{k}}}{\omega_{n'\mathbf{k}}} \quad (20)$$

The coefficients  $B_{\alpha\beta} = 0$  vanish identically only if occupation numbers of the photoexcited carriers remain invariant under time reversal symmetry  $[f_{n\mathbf{k}} = f_{n-\mathbf{k}}]$ . For clean semiconductor, the coefficients  $A_{\alpha\beta}$  also vanish, because for filled bands, occupation numbers  $f_{n\mathbf{k}}^0 = \{0, 1\}$ , independently on  $\mathbf{k}$ . However  $A_{\alpha\beta}$  does not vanish because in general photoexcited carriers are non-uniformly distributed over the Brillouin zone, so that  $\chi_{\alpha\beta}$  does diverge when  $\omega \rightarrow 0$ . Introducing a dielectric tensor of the photoexcited solid

$$\epsilon_{\alpha\beta}(\omega) = \delta_{\alpha\beta} + 4\pi\chi_{\alpha\beta}(\omega), \quad (21)$$

the Maxwell's equation  $\epsilon_{\alpha\beta}(\omega)A_{\beta}(\omega) = 0$  possesses nontrivial solution when  $\det \epsilon(\omega) = 0$ , which specifies the collective eigenmodes of the polarization. The dielectric tensor can be split into isotropic part and a traceless part associated with the optical anisotropy of the solid

$$\epsilon_{\alpha\beta}(\omega) = \epsilon(\omega)\delta_{\alpha\beta} + \eta_{\alpha\beta}(\omega) \quad (22)$$



where  $\epsilon(\omega) = \text{tr}\epsilon(\omega)/3$  is the dielectric function. Assuming that that optical anisotropy of the photoexcited solid is weak, using Eq.(16), neglecting the interband contribution of  $B$  coefficients and introducing a background dielectric function

$$\epsilon_b = 1 + \frac{4\pi}{3}\text{tr}\mathbf{C} \quad (23)$$

which exhibits weak frequency dependence for subbandgap excitation, the dielectric function can be recast into the classical Drude form

$$\epsilon(\omega) = \epsilon_b \left( 1 - \frac{\omega_p^2}{\omega^2} \right) \quad (24)$$

with the definition of screened plasma oscillation frequency of free carriers

$$\omega_p = \left( \frac{4\pi n_0}{m^* \epsilon_b} \right)^{1/2} \quad (25)$$

and a band-averaged inverse effective mass of an electron-hole pair

$$\frac{1}{m^*} = \frac{1}{n_0} \sum_n \int_{\text{BZ}} \frac{d^3\mathbf{k}}{4\pi^3} f_{n\mathbf{k}} \frac{1}{3} \text{tr} \left( \frac{1}{m_{n\mathbf{k}}^*} \right) \quad (26)$$

The intensity and fluence dependence of the dielectric function of the pumped solid enters via the effective mass parameter and the Pauli-blocking factors  $f_{n\mathbf{k}} - f_{n'\mathbf{k}}$ .

### III. NUMERICAL RESULTS AND DISCUSSION

The static energy-band structure of silicon along the  $\Delta$  and  $\Lambda$  lines in the Brillouin zone is shown in Fig. 1. The pseudopotential model reproduces quantitatively the principal energy gaps and the optical properties of silicon. The location of the conduction band minimum at  $\mathbf{k} = (0.8, 0, 0)$  relative to the valence band top at the  $\Gamma$  point, specifies the threshold for indirect transitions  $\approx 1$  eV. The threshold for direct transitions is assigned to the  $\Gamma_{25} \rightarrow \Gamma_{15}$  energy gap (3.2 eV). In the practical calculations<sup>56,57</sup>, dense sampling of the Brillouin zone was made by a Monte Carlo method using 2500 quasi-randomly generated  $\mathbf{k}$ -points (points were generated from three-dimensional Sobol sequence in a cube of edge length  $4\pi/a_0$ ,<sup>55</sup>);  $N=20$  bands were included in the expansion of the wave-packet over static Bloch orbitals, with 4 valence and 16 conduction bands. The Cayley transformation was applied to propagate the Bloch wave-functions forward in time for small equidistant time steps  $\delta t \approx 1$  attosecond

$$|\psi_{v\mathbf{k}}(t + \delta t)\rangle = [1 - iH(\mathbf{k}, t)\delta/2]^{-1}[1 + iH(\mathbf{k}, t)\delta/2]|\psi_{v\mathbf{k}}(t)\rangle \quad (27)$$

where  $H(\mathbf{k}, t) = \exp(i\mathbf{k} \cdot \mathbf{r})H(t)\exp(-i\mathbf{k} \cdot \mathbf{r})$ , next the single-particle density matrix is evaluated

$$\rho_{nn'\mathbf{k}}(t) = \sum_v \langle n\mathbf{k} | \psi_{v\mathbf{k}}(t) \rangle \langle \psi_{v\mathbf{k}}(t) | n'\mathbf{k} \rangle \quad (28)$$

and the current density

$$\mathbf{J}(t) = \text{tr}[\rho(t)\mathbf{v}(t)] \quad (29)$$

is used to update the macroscopic vector potential according to

$$\mathbf{A}_{\text{ind}}(t + \delta t) = 2\mathbf{A}_{\text{ind}}(t) - \mathbf{A}_{\text{ind}}(t - \delta t) + 4\pi\mathbf{J}(t)\delta t^2 \quad (30)$$

### A. Excitation by a single pulse

Fig.2 (a-b) show the laser-induced AC currents in bulk silicon for three different laser intensities  $I = 3 \times 10^{13} \text{ W/cm}^2$ ,  $I = 1.2 \times 10^{14} \text{ W/cm}^2$  and  $I = 6 \times 10^{14} \text{ W/cm}^2$ . The laser wavelength was set to 800 nm (photon energy  $\hbar\omega = 1.55 \text{ eV}$ ) and the polarization vector  $\mathbf{e}$  is pointing along the [001] direction. Fig.2a gives the component of the total photocurrent in direction of the laser polarization. The induced currents are nearly in phase and follow the Gaussian profile and periodicity of the applied laser vector potential. As the intensity of the pulse increases, the amplitude of the current also increases. Fig.2b also shows the time evolution and intensity dependence of the intraband part of the photocurrent, the interband part exhibits similar temporal variation, but is completely out of phase with the intraband current during the whole time evolution. For the lowest laser intensity shown,  $I = 3 \times 10^{13} \text{ W/cm}^2$ , the laser generates completely reversible currents inside the bulk. For the increased laser intensity  $I = 1.2 \times 10^{14} \text{ W/cm}^2$ , an intensity-dependent phase shift of the current relative to the applied laser field accumulates in between the middle and the end of the pulse. Interband motion of charge carriers persists long after the end of the pulse, indicating that irreversible and highly efficient transfer of laser energy to electrons has occurred. For the highest intensity shown,  $I = 6 \times 10^{14} \text{ W/cm}^2$ , the photocurrent builds up rapidly on the leading part of the pulse, near and after the pulse peak the non-linear phase shift stabilizes and the applied electric field lags behind the current by  $\pi/2$ .

Fig. 3(a-c) show the temporal profile of the applied and total electric fields, corresponding to the three laser intensities discussed above. Fig.3 (d-f) and Figs. 3(g-i) present the associated time evolution of the conduction electron density and absorbed energy per Si

atom, respectively. At low intensities, Fig.(3(a)), the total and applied electric fields are in phase during the whole time evolution and dielectric response of electrons is exhibited, the electric field is screened inside the bulk  $\mathbf{E} = \mathbf{E}_{\text{ext}}/\epsilon$  with  $\epsilon \approx 12$  - the static dielectric constant of Si. The peak electric field strength inside the bulk reaches  $0.1 \text{ V/\AA}$ , which is relatively weak to produce high level of electronic excitation. The conduction electron density in Fig.(3(d)) exhibits temporal oscillations following the periodicity of driving laser field due to virtual transitions into of and out the conduction band. Real electron-hole are born at the extrema of the laser field by perturbative three- and four-photon photon transitions from the valence into the conduction band. Near the peak of the pulse the transient number density of electron-hole pairs reaches  $10^{21} \text{ cm}^{-3}$ , this number is reduced subsequently mainly due to the disappearance of virtual population. The final photoelectron yield does not exceed  $10^{20} \text{ cm}^{-3}$ . Quite similarly the time evolution of the absorbed energy in Fig.(3(g)) displays rapid transient oscillations due to continuous population and depopulation of the conduction band during each half-cycle, the energy gained during each half-cycle is almost fully returned back to the field. The total energy irreversible deposited onto electrons after the end of the pulse is well below  $0.01 \text{ eV/atom}$ .

When the laser intensity is increased to  $I = 1.2 \times 10^{14} \text{ W/cm}^2$ , Fig.(3(b)), progressive phase lag of the applied relative to the total electric field occurs in between the middle and the end of the pulse. Few femtoseconds after the peak of the applied laser field, the peak field strength inside the bulk reaches  $0.3 \text{ V/\AA}$ , this delayed response of the non-linear polarization manifests in self-sustained electric field with strength  $0.1 \text{ V/\AA}$  long after conclusion of the pulse. In this regime, Fig.(3(e)), photoionization is very efficient, and when about 5% of the valence electrons are ionized by multiphoton and tunnel transitions, collective plasma oscillations of the electron gas emerge. The plasma oscillation frequency nearly matches the frequency of the applied laser pulse. The coherent oscillation in the population of the conduction bands is sustained by the non-linear polarization long after the end of the pulse. The electronic excitation energy in Fig.(3(h)) increases in cumulative manner following the successive cycles of the driver pulse. The amount of energy irreversibly deposited onto electrons rises above the thermal melting threshold of Si (1687 Kelvins) slightly after the pulse peak. Few femtoseconds later, energy deposition saturates and reaches  $0.5 \text{ eV/atom}$  that exceeds a few times the thermal melting threshold.

When the laser intensity is increased further to  $I = 6 \times 10^{14} \text{ W/cm}^2$ , Fig.(3(c)), the applied

field lags behind the total electric field on the rising edge of the pulse, which results in shock-like deposition of energy to electrons Fig.(3(i)). Their number density in Fig.(3(f)) increases rapidly by more than two orders of magnitude for few cycles on the rising edge of the driver pulse. Slightly before the pulse peak, the total and applied electric fields are completely out of phase, when further transfer of energy to electrons is suppressed. The number of conduction electrons and the excitation energy saturate to  $2 \times 10^{22} \text{ cm}^{-3}$  and 3 eV/atom, respectively. For such high level of excitation, metallic response of the photoexcited Si is clearly exhibited, the lack of density oscillations after the end of the pulse is because the plasma frequency shifts above the laser frequency and conduction electrons screen out the electric field inside the bulk.

To analyze this further, in Fig.(4(a)) we plot the Fourier transform of the pulsed electric field. For low laser intensity, the distribution is centered at the laser wavelength ( $\approx 800 \text{ nm}$ ) and exhibits Gaussian profile. The spectral distribution gains large amplitude and becomes narrower when the laser intensity is increased into the region of the plasmon resonance with  $I \approx 10^{14} \text{ W/cm}^2$ . For the highest shown intensity  $6 \times 10^{13} \text{ W/cm}^2$ , the distribution broadens in wavelength resulting in contraction of the pulse length in the time domain. The central wavelength undergoes a progressive blue shift, such that the plasma frequency moves off resonance with the applied laser. The spectral phase of the pulsed electric field relative to the photocurrent is also shown in Fig.(4(b)). For low intensity, the spectral phase shift is close to  $\pi/2$  in the absorption region and dielectric response is exhibited. As the laser intensity increases into the region of the plasmon resonance, the spectral components on the red side of the central wavelength are in phase with the photocurrent, such that electrons gain much energy by interacting with the laser. However because of the dispersion of the spectral phase in the absorption region, this contribution is partially cancelled by interactions with shorter wavelengths on the blue side of the central wavelength. The variation of the spectral phase also causes a time delay of the envelope of the pulsed electric field relative to applied laser (cf. also Fig.(3(b))). At the highest intensity shown, the phase stabilizes in the absorption region: the pulsed electric field and the current are nearly in phase, such that nonlinear absorption and energy transfer to electrons is greatly enhanced.

In Fig.(5(a-b)), we plot the dependence of the total absorbed energy and conduction electron density on the laser intensity for two different laser polarization directions - [001] and [111] directions. In the low intensity regime with  $I < 10^{14} \text{ W/cm}^2$ , perturbative superlinear

scaling trend is exhibited with  $\Delta E \sim I^3$  with corresponding to dominant three-photon absorption process. For higher intensities  $I > 10^{14}$  W/cm<sup>2</sup>, a qualitative change in electron dynamics occurs with sublinear trend  $\Delta E \sim I^{1/2}$  and  $n \sim I^{1/3}$ . This regime corresponds to high level of electronic excitation, when more than 5 % of valence electrons are ionized and the absorbed energy  $\Delta E > 0.1$  eV/atom is above the thermal melting threshold of Si. Similar sublinear scaling trend of the photocarrier density in silicon in the regime of high excitation was measured in Ref.<sup>58</sup>. The absorbed energy depends also sensitively on the laser polarization direction: in the low intensity regime, energy is more efficiently deposited for laser linearly polarized along the [111] direction as compared to the [001] direction. This sensitivity is enhanced in the region of the plasmon resonance near  $I \approx 10^{14}$  W/cm<sup>2</sup>, e.g. 0.7 eV/atom are deposited for laser polarized along the [111] direction, 0.2 eV/atom are deposited when the polarization vector points along the [001] direction.

Further details on the excitation mechanism are included in the energy distribution of photoexcited electrons. The density of conduction band states is characterized by two broad peaks with energies 2.5 and 4 eV above the valence band maximum, which are associated with 3 and 4-photon transitions. The intensity of the distribution increases with the increase of the laser intensity and high energy tail emerges. The effect of Pauli blocking is clearly exhibited in the saturation of the density of states in the low energy part of the distribution. Thus band filling results in altered probabilities for interband excitation and saturation of photoionization at high intensity.

The momentum-resolved distribution function of conduction electrons  $f(\mathbf{k}) = \sum_c f_c(\mathbf{k})$  is also shown in Fig.7, for the three different laser intensities, Fig.7(a-c) correspond to laser linearly polarized along the [001] direction and Fig.7 refer to the [111] direction. Noticeably the photocarrier distribution is highly non-uniform and anisotropic in the Brillouin zone. For low intensity  $I = 3 \times 10^{13}$  W/cm<sup>2</sup>, small fraction of valence electrons are promoted into the conduction bands with occupation numbers of order  $10^{-3}$  (cf. Fig.7(a,d)). More electrons emerge along the  $\Lambda$  line for laser polarized along [001] direction, Fig.7a. When the laser polarization vector points in the [111] direction, Fig.7d, spectral structure forms near the  $\Gamma$  point, and a broad shoulder of electrons emerges along the  $\Delta$  line and near the X valleys. As the laser intensity increases to  $I = 1.2 \times 10^{14}$  W/cm<sup>2</sup>, occupation of conduction bands increases substantially and the distribution broadens in the Brillouin zone, (cf. Fig.7(b,e)). Band and state filling is characterized by sharp peaks associated with specific points in

the Brillouin zone . The high degree of occupation of conduction bands with occupation numbers  $\sim 1$  makes evident the significance of Pauli blocking in this regime. For the highest intensity shown  $I = 6 \times 10^{14} \text{ W/cm}^2$  (in Fig.7(c,f)), the degree of population inversion does not change much on average, instead altered probabilities for interband excitation due to Pauli blocking result in redistribution of carriers over states.

Using these distributions we compute the optical constants of the photoexcited Si according to Eqs.19 and 17. Results are shown in Fig.8(a-b) for laser linearly polarized along the [001] direction. where the variation of the dielectric constant and the optical reflectivity as a function of the laser fluence are shown. For low fluences, below  $0.1 \text{ J/cm}^2$ , the reflectivity is nearly constant  $R = 0.3$  and dielectric response is exhibited. The reflectivity decreases with the increase of the fluence and attains minimum around  $0.7 \text{ J/cm}^2$ . Above that fluence, the reflectivity increases rapidly and reaches  $R \approx 0.4$  at  $1.3 \text{ J/cm}^2$ . This behavior reproduces qualitatively the main features of the measured evolution of reflectivity with fluence<sup>16</sup>. The principal contribution near the minimum of the reflectivity curve is due to band filling and interband transitions, resulting in sensitive and non-monotonic fluence dependence of the background dielectric constant  $\epsilon_b$ . The effective mass  $m^*$  of free carriers exhibits moderate fluence dependence, and it decreases monotonically with increase of the fluence. The flattening of the slope of the reflectivity rise above the minimum is also in very good agreement with the measured data. This flattening is due to competition of band filling, Pauli blocking and free-carrier contribution. In that region, the interband contribution increases due to redistribution of carriers over states, since free-carrier polarization gives always negative contribution it reduces the high polarizability of the pumped silicon. When the laser frequency matches the screened plasma frequency near  $1.4 \text{ J/cm}^2$  (laser intensity  $1.2 \times 10^{14} \text{ W/cm}^2$ ), the free-carrier response dominates, the dielectric constant vanishes and electron-hole pairs exhibit a coherent plasma oscillation.

## B. Excitation by double pulse sequence

To investigate the nonlinear response of the photoexcited plasma to strong laser field we apply a second identical pulse after photoexcitation of Si by the first pulse. While for low intensities, Fig.9(a,c), the effect of two pulses is additive in terms of absorbed energy and photoelectron density, strong effect of enhancement in terms of absorbed energy occurs

for laser intensity in the region of the plasmon resonance in Fig.9(b,d): the second pulse deposits two times more energy than the first one. That is because the self-electric field of the plasmon excited by the first pulse interferes with the electric field of the second applied pulse, resulting in highly efficient transfer of energy to electrons on the rising edge of the second pulse. When the laser intensity is increased, Fig.9(c,e) the laser oscillation frequency shifts below the plasma frequency, such that the photoexcited solid shows metal-like response and becomes reflective for the incident irradiation, such that the electric field of the second pulse is screened out and large portion of its energy is reflected away.

#### IV. CONCLUSION

In summary we have investigated the ultrafast photoexcitation and plasma formation in crystalline silicon interacting with 12fs near infrared laser pulse. For peak laser intensities near and above  $10^{14}$  W/cm<sup>2</sup>, photoionization creates dense plasma of electron-hole pairs and strongly absorbing state of silicon for near infrared laser wavelengths, with deposited energies a few times exceeding the thermal melting threshold. This state may be considered as a precursor to ultrafast phase transition and melting of silicon, as reported experimentally using femtosecond lasers. The linear response of the laser-excited state was analysed in terms of interband and free-carrier responses. The fluence dependence of the optical reflectivity of the pumped silicon reproduces qualitatively the principal features observed in the experiments. We have demonstrated the relative importance between band filling effects and Pauli blocking and free-carrier Drude response. In this paper, the optical anisotropy of the photoexcited silicon was considered as weak, the effects like optically induced birefringence may be subject to our follow-up paper.

With regard to the formation and properties of laser-induced periodic surface structures on Si surfaces, the non-linear response of the photoexcited silicon was investigated by exposing the crystal to a sequence of two temporary non-overlapping strong ultrashort laser pulses. Depending sensitively on the laser intensity, highly efficient deposition of the laser energy is demonstrated resulting from the interference of the incident laser irradiation with the excited bulk plasmon excitations.

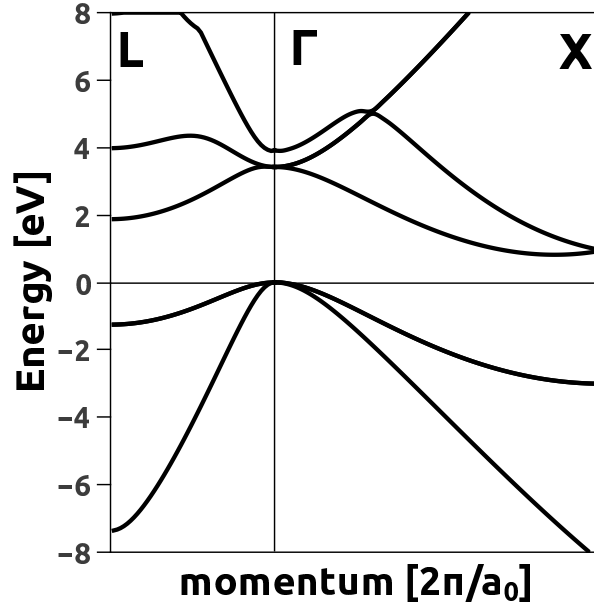


FIG. 1. Static band structure of silicon along the  $\Delta$  and  $\Lambda$  lines in the Brillouin zone. The crystal momentum is measured in units  $2\pi/a_0$ , where  $a_0 = 5.43$  Å is the bulk lattice constant.

## ACKNOWLEDGEMENTS

This material is based upon work supported by the Air Force Office of Scientific Research under award number FA9550-19-1-7003. Cost action CA17126 is acknowledged. (B.O.) also acknowledges financial support from the Bulgarian National Science Fund under Contract No. 08-17.

- 
- <sup>1</sup> C. V. Shank, Y. Yen, and C. Hirlimann, Phys. Rev. Lett. **51**, 900 (1983).
  - <sup>2</sup> H. W. K. Tom, G. D. Aumiller and C. H. Brito-Cruz, Phys. Rev. Lett. **60**, 1438 (1988).
  - <sup>3</sup> K. Sokolowski-Tinten, J. Bialkowski and D. von der Linde, Phys. Rev. B **51**, 14186 (1995).
  - <sup>4</sup> E. N. Glezer, Y. Siegal, L. Huang, E. Mazur, Phys. Rev. B **51**, 6959 (1995).
  - <sup>5</sup> Y. Siegal, E. N. Glezer, L. Huang, and E. Mazur, Annu. Rev. Mater. Sci. **25**, 223 (1995).
  - <sup>6</sup> L. Huang, J. P. Callan, E. N. Glezer, and E. Mazur, Phys. Rev. Lett. **80**, 185 (1997).
  - <sup>7</sup> A. Rousse, C. Rischel, S. Fourmaux, I. Uschmann, S. Sebban, G. Grillon, P. Balcou, E. Förster, J. P. Geindre, P. Audebert, and J. C. Gauthier, Nature, **410**, 65 (2001).



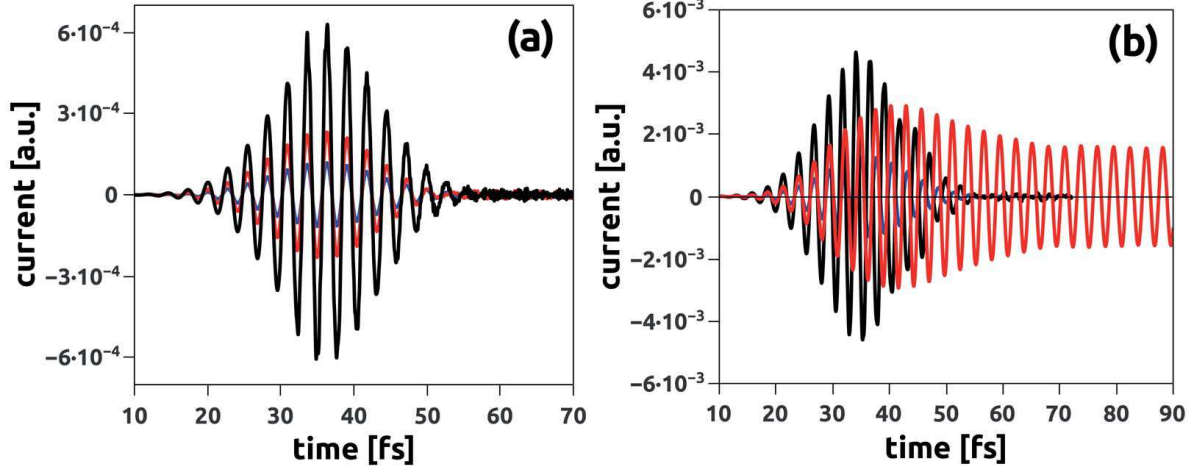


FIG. 2. (a) Time evolution of the photoinduced current in bulk silicon subjected to pulsed laser with peak intensity  $I = 3 \times 10^{13} \text{ W/cm}^2$  (dotted line),  $I = 1.2 \times 10^{14} \text{ W/cm}^2$  (dashed line) and  $I = 6 \times 10^{14} \text{ W/cm}^2$  (solid line). (b) Time evolution of the interband current in bulk silicon for laser intensity  $I = 3 \times 10^{13} \text{ W/cm}^2$  (dotted line),  $I = 1.2 \times 10^{14} \text{ W/cm}^2$  (dashed line) and  $I = 6 \times 10^{14} \text{ W/cm}^2$  (solid line). In Fig.(a-b) the pulse is linearly polarized along the [001] direction, the laser wavelength is 800 nm and the pulse duration is 12fs.

- <sup>8</sup> A. M.-T. Kim, J. P. Callan, C. A. D. Roeser, and E. Mazur, Phys. Rev. B **66**, 245203 (2002).
- <sup>9</sup> K. Sokolowski-Tinten, C. Blome, J. Blums, A. Cavalleri, C. Dietrich, A. Tarasevitch, I. Uschmann, E. Förster, M. Kammler, M. Horn-von-Hoegen and D. von der Linde, Nature **422**, 287 (2003).
- <sup>10</sup> J. Bonse, S. M. Wiggins, and J. Solis, J. Appl. Phys. **96**, 2628 (2004).
- <sup>11</sup> M. Harb, R. Ernstorfer, C. T. Hebeisen, G. Sciaini, W. Peng, T. Dartigalongue, M. A. Eriksson, M. G. Lagally, S. G. Kruglik, and R. J. Dwayne Miller, Phys. Rev. Lett. **100**, 155504 (2008).
- <sup>12</sup> S. Das Sarma and J. R. Senna, Phys. Rev. B **49**, 2443 (1994).
- <sup>13</sup> P. Stampfli and K. H. Bennemann, Phys. Rev. B **42**, 7163 (1990); P. Stampfli and K. H. Bennemann, Phys. Rev. B **46**, 10686 (1992); P. Stampfli and K. H. Bennemann, Phys. Rev. B **49**, 7299 (1999).
- <sup>14</sup> P. L. Silvestrelli, A. Alavi, M. Parrinello, and D. Frenkel, Phys. Rev. Lett. **77**, 3149 (1996).
- <sup>15</sup> R. Darkins, P.-W. Ma, S. T. Murphy, D. M. Duffy, Phys. Rev. B **98**, 024304 (2018).
- <sup>16</sup> K. Sokolowski-Tinten, D. von der Linde, Phys. Rev. B **61**, 2643 (2000).

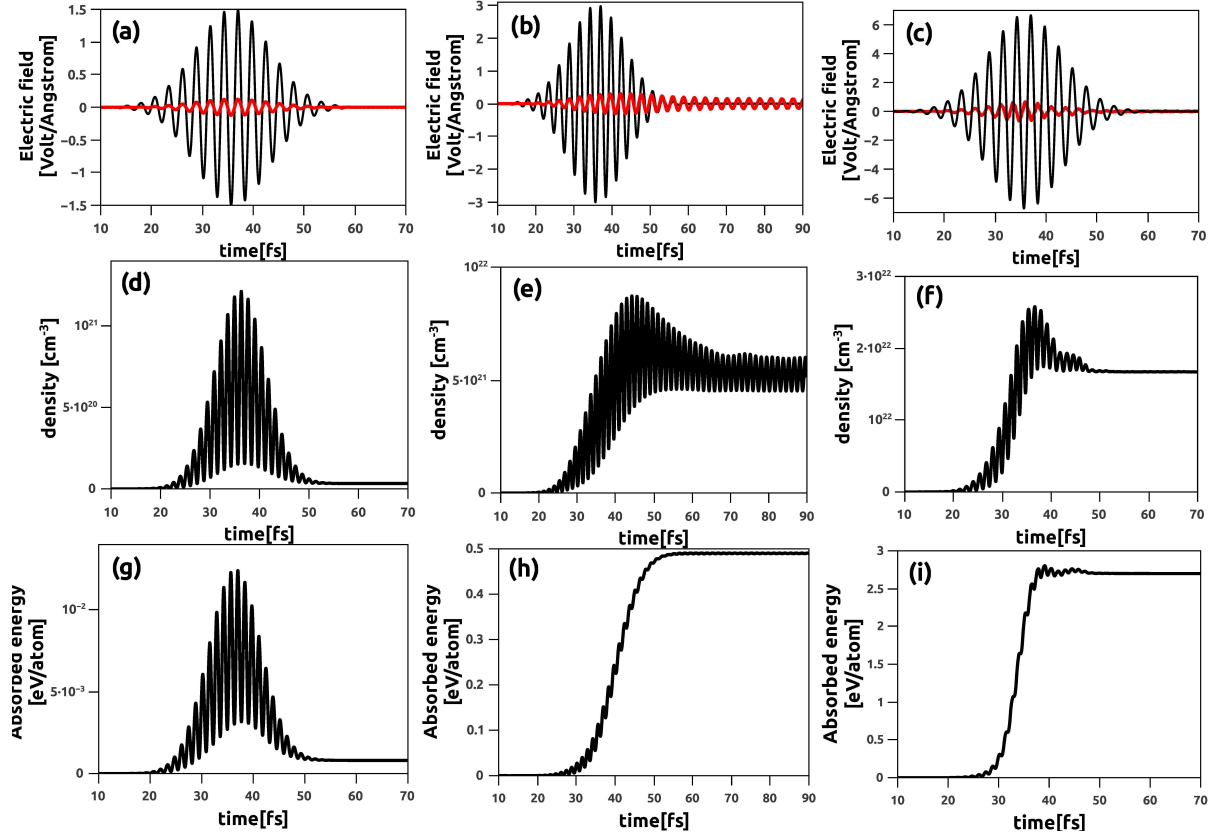


FIG. 3. (a-c) Time evolution of the pulsed electric field (in V/Å) of the applied laser (dashed line) and the total electric field (in V/Å) (solid line) in bulk silicon. The laser intensity at the pulse peak is  $3 \times 10^{13}$  W/cm<sup>2</sup> in (a),  $1.2 \times 10^{14}$  W/cm<sup>2</sup> in (b) and is  $6 \times 10^{14}$  W/cm<sup>2</sup> in (c). Fig.(d-f) time evolution of the conduction electron density (in cm<sup>-3</sup>) in bulk silicon. Fig.(g-i) give the time evolution of the absorbed energy in eV per Si atom. The laser is linearly polarized along the [001] direction, the laser wavelength is 800 nm and the pulse duration is 12fs.

- <sup>17</sup> D. Hulin, M. Combescot, J. Bok, A. Migus et al., Phys. Rev. Lett. **52**, 1998 (1984)
- <sup>18</sup> J. Frigerio, A. Ballabio, G. Isella, E. Sakat, G. Pellegrini, P. Biagioni, M. Bollani, E. Napolitani, C. Manganeli, M. Virgilio and A. Grupp, Phys. Rev. B **94**, 085202 (2016).
- <sup>19</sup> B. Rethfeld, Phys. Rev. Lett. **92**, 187401 (2004).
- <sup>20</sup> N. Medvedev and B. Rethfeld, J. Appl. Phys. **108**, 103112 (2010).
- <sup>21</sup> L. X. Benedict, Phys. Rev. B **63**, 075202 (2001).
- <sup>22</sup> C. D. Spataru, L. X. Benedict, S. G. Louie, Phys. Rev. B **69**, 205204 (2004).

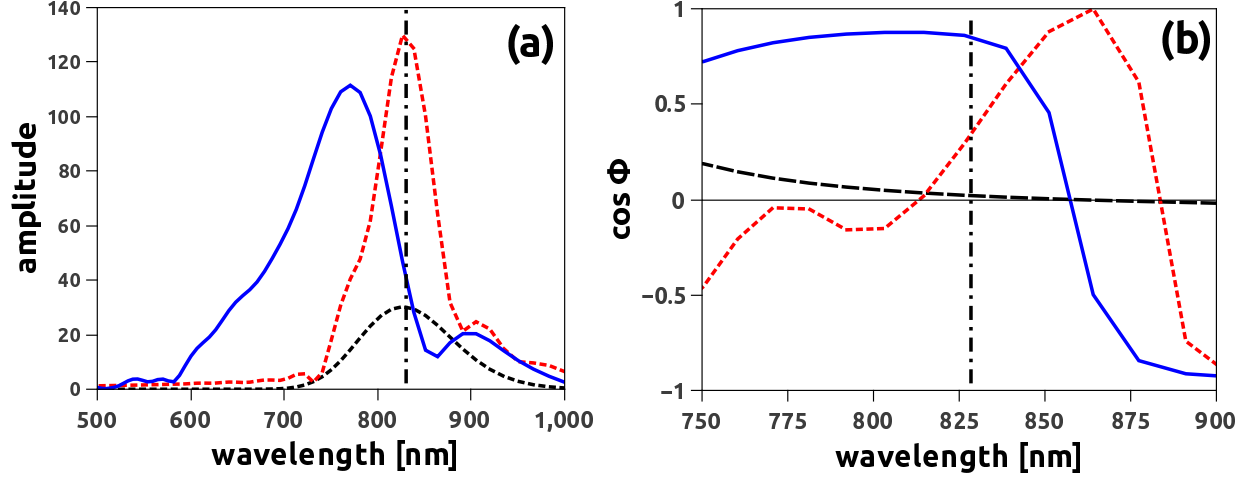


FIG. 4. Fig.(a) Laser intensity dependence of the spectral amplitude and (b) (cosine of) the spectral phase of the pulsed electric field inside bulk silicon. Different curves correspond to different laser intensities:  $I = 3 \times 10^{13} \text{ W/cm}^2$  (dashed line),  $I = 1.2 \times 10^{14} \text{ W/cm}^2$  (dotted line) and  $I = 6 \times 10^{14} \text{ W/cm}^2$  (solid line). In Fig.(a-b) the laser is linearly polarized along the [001] direction, the laser wavelength is 800 nm and the pulse duration is 12fs.

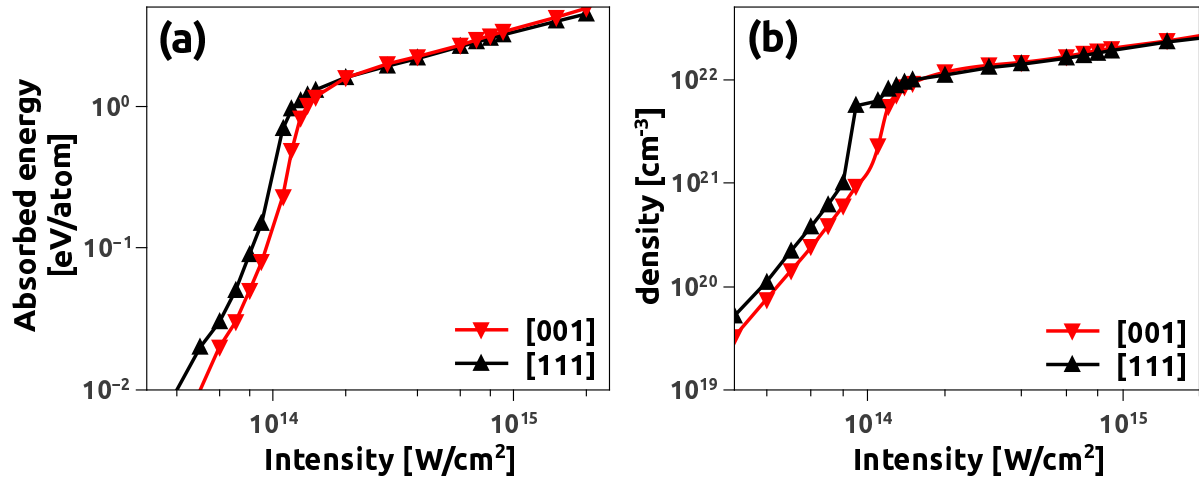


FIG. 5. Peak laser intensity dependence of the absorbed energy per atom (in eV) (a) and (b) the conduction electron density (in  $\text{cm}^{-3}$ ) in bulk silicon subjected to 12fs pulsed laser irradiation with wavelength 800 nm. Upper triangles - laser is linearly polarized along the [111] direction, lower triangles - laser linearly polarized along [001] direction.

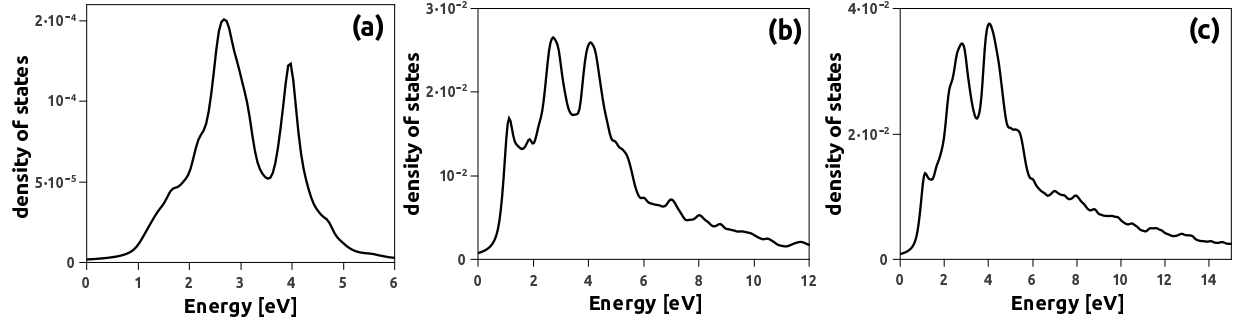


FIG. 6. Density of conduction electron states in silicon after excitation by 12fs near-infrared laser with wavelength 800 nm. The laser intensity is: (a)  $I = 3 \times 10^{13}$  W/cm<sup>2</sup>, (b)  $I = 1.2 \times 10^{14}$  W/cm<sup>2</sup> and (c)  $I = 6 \times 10^{14}$  W/cm<sup>2</sup>. The laser is linearly polarized along the [001] direction.

- <sup>23</sup> T. Otobe, M. Yamagiwa, J.-I. Iwata, K. Yabana, T. Nakatsukasa, and G. F. Bertsch, Phys. Rev. B **77**, 165104 (2008).
- <sup>24</sup> T. Otobe, K. Yabana and J.-I. Iwata, J. Phys. Cond. Matt. **21**, 064224 (2009).
- <sup>25</sup> K. Yabana, T. Sugiyama, Y. Shinohara, T. Otobe, and G. F. Bertsch, Phys. Rev. B **85**, 045134 (2012).
- <sup>26</sup> S. A. Sato, K. Yabana, Y. Shinohara, T. Otobe, and G. F. Bertsch, Phys. Rev. B **89**, 064304 (2014).
- <sup>27</sup> S. A. Sato, Y. Shinohara, T. Otobe, and K. Yabana, Phys. Rev. B **90**, 174303 (2014).
- <sup>28</sup> F. Krausz and M. Ivanov, Rev. Mod. Phys. **81**, 163 (2009).
- <sup>29</sup> M. I. Stockman, K. Kneipp, S. I. Bozhevolnyi, S. Saha, A. Dutta, J. Ndukaife, N. Kinsey, H. Reddy, U. Guler, V. M. Shalaev, J. Opt. **20** 043001, (2018).
- <sup>30</sup> A. Sommer, E. M. Bothschafter, S. A. Sato, C. Jakubeit, T. Latka, O. Razskazovskaya, H. Fattahi, M. Jobst, W. Schweinberger, V. Shirvanyan, V. S. Yakovlev, R. Kienberger, K. Yabana, N. Karpowicz, M. Schultze and F. Krausz, Nature **534**, 86 (2016).
- <sup>31</sup> M. Schultze, K. Ramasesha, C. D. Pemmaraju, S. A. Sato, D. Whitmore, A. Gandman, J. S. Prell, L. J. Borja, D. Prendergast, K. Yabana and D. M. Neumark, Science **346**, 1348 (2014).
- <sup>32</sup> F. Krausz, M. I. Stockman, Nat. Photonics **8**, 205 (2014).
- <sup>33</sup> S. Han, L. Ortmann, H. Kim, Y. W. Kim, T. Oka, A. Chacon, B. Doran, M. Ciappina, M. Lewenstein, S.-W. Kim, S. Kim and A. S. Landsman, Nature Communications, **10**, 3272 (2019).

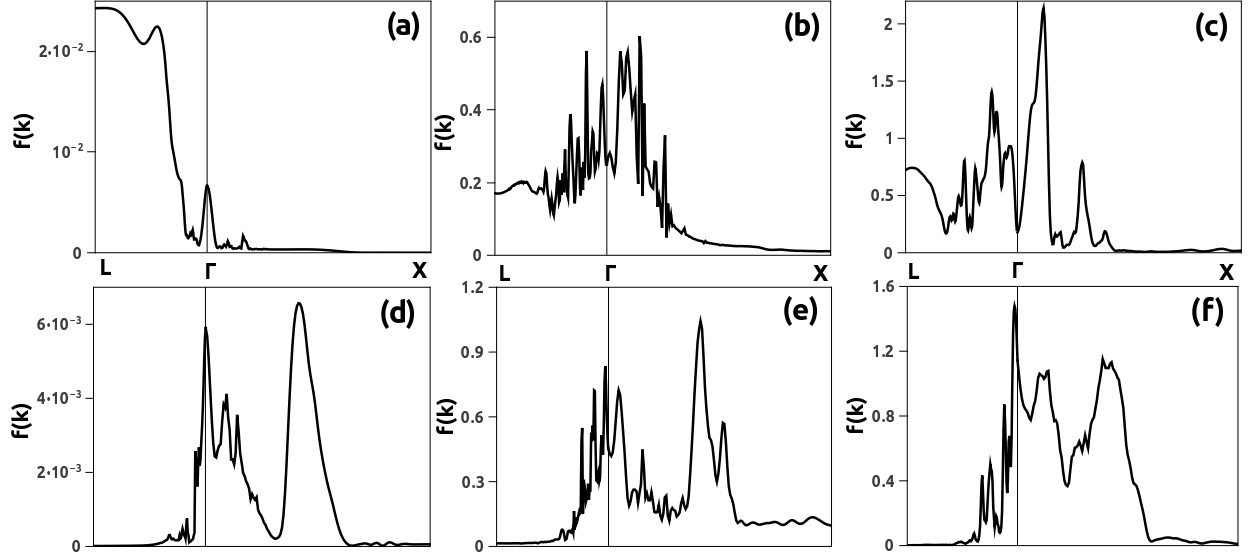


FIG. 7. Crystal momentum distribution of conduction electrons in silicon after excitation by 12fs near-infrared laser pulse with wavelength 800 nm. In Fig.(a-c) the laser is linearly polarized along the [001] direction. In Fig.(d-f) the laser polarization vector points along the [111] direction. The peak laser intensity is:  $I = 3 \times 10^{13} \text{ W/cm}^2$  in Fig.(a) and Fig.(d),  $I = 1.2 \times 10^{14} \text{ W/cm}^2$  in Fig.(b) and Fig.(e), and  $I = 6 \times 10^{14} \text{ W/cm}^2$  in Fig.(c) and Fig.(f).

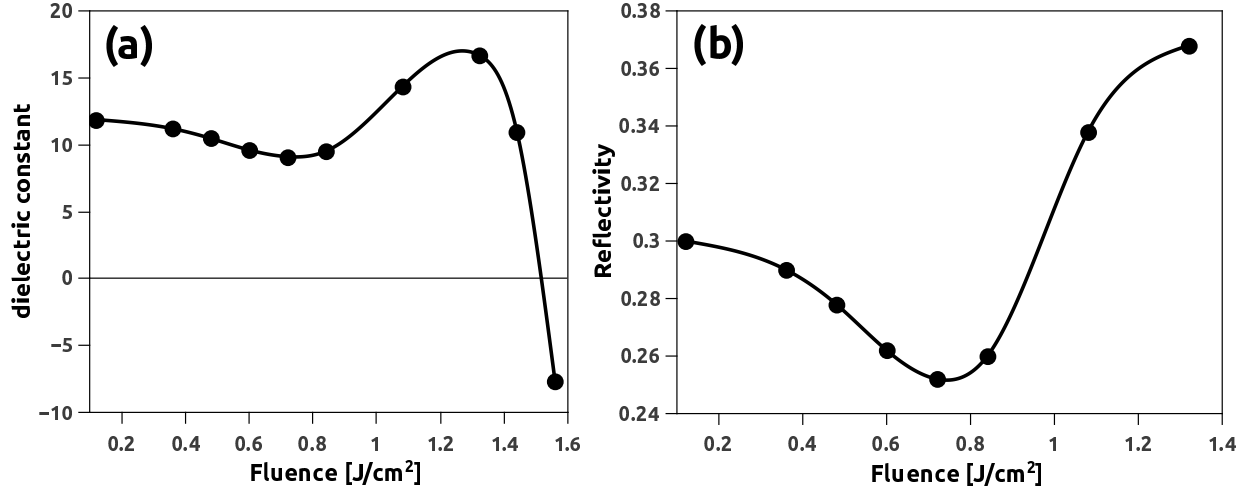


FIG. 8. (a) Laser fluence dependence of dielectric constant of the photoexcited silicon and Fig. (b) gives the change of optical reflectivity as a function of the fluence. In Fig.(a-b) the laser is linearly polarized along the [001] direction, the laser wavelength is 800 nm and the pulse duration is 12fs.

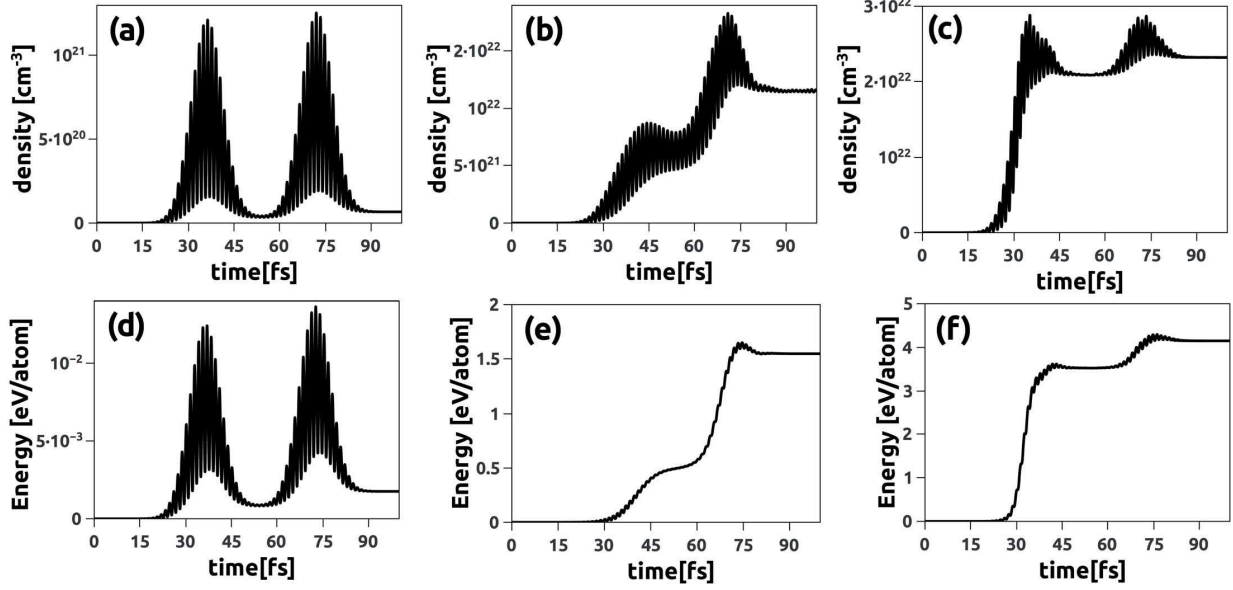


FIG. 9. (a-c) Time-evolution of the conduction electron density (in  $\text{cm}^{-3}$ ) and (d-f) absorbed energy per atom (in eV) in bulk silicon subjected to a sequence of two identical non-overlapping 12fs near-infrared pulses with wavelength 800 nm. The peak laser intensity  $I = 3 \times 10^{13} \text{ W/cm}^2$  in Fig.(a) and Fig.(d),  $I = 1.2 \times 10^{14} \text{ W/cm}^2$  in Fig.(b) and Fig.(e), and  $I = 6 \times 10^{14} \text{ W/cm}^2$  in Fig.(c) and Fig.(f).

- <sup>34</sup> D. Du, X. Liu, G. Korn, J. Squier, G. Mourou, Appl. Phys. Lett. **64**, 3071 (1994).
- <sup>35</sup> B. C. Stuart, M. D. Veit, S. Herman, A. M. Rubenchik, B. W. Shore, M. D. Perry, Phys. Rev. B **53**, 1749 (1996).
- <sup>36</sup> W. Kautek, J. Krüger, M. Lenzner, S. Sartania, Ch. Spielmann, F. Krausz, Appl. Phys. Lett. **69**, 3146 (1996).
- <sup>37</sup> M. Lenzner, J. Krüger, S. Sartania, Z. Cheng, Ch. Spielmann, G. Mourou, W. Kautek, and F. Krausz, Phys. Rev. Lett. **80**, 4076 (1998).
- <sup>38</sup> M. Li, S. Menon, J. P. Nibarger, and G. N. Gibson, Phys. Rev. Lett. **82**, 2394 (1999).
- <sup>39</sup> T. Apostolova and Y. Hahn, Journal of Applied Physics **88**, 1024 (2000).
- <sup>40</sup> T. Apostolova, D. H. Huang, P. M. Alsing, J. McIver, D. A. Cardimona, Phys. Rev. B. **66**, 075208 (2002).
- <sup>41</sup> P. P. Rajeev, M. Gertsvolf, P. B. Corkum, and D. M. Rayner, Phys. Rev. Lett. **102**, 083001 (2009).

- <sup>42</sup> P. A. Zhokhov and A. M. Zheltikov, Sci. Rep., **8**, 1824 (2018).
- <sup>43</sup> J. Reif, Laser-Surface Interactions for New Materials Production. Springer, Berlin, Heidelberg, 19, 2010.
- <sup>44</sup> E. G. Gamaly, A. V. Rode, and B. Luther-Davies, Physics of Plasmas **9**, 949 (2002)
- <sup>45</sup> E. G. Gamaly, Phys. Rep. **508**, 91 (2011)
- <sup>46</sup> I. Mirza, N. M. Bulgakova, J. Tomášťik, V. Michálek, O. Haderka, L. Fekete, and T. Mocek, Scientific reports, **6**, 39133, (2016)
- <sup>47</sup> J. Bonse, A. Rosenfeld, J. Kruger, J. Appl.Phys. **106**, 104910 (2009).
- <sup>48</sup> G. D. Tsibidis, M. Barberoglou, P. A. Loukakos, E. Stratakis, C. Fotakis, Phys.Rev B **86**, 115316 (2012).
- <sup>49</sup> D. Ashkenasi, A. Rosenfeld, H. Varel, M. Wahmer, E. E. B. Campbell, Appl. Surf. Sci. **120**, 65 (1997)
- <sup>50</sup> G. Miyaji, M. Hagiya, and K. Miyazaki,Phys. Rev. B **96**, 045122 (2017)
- <sup>51</sup> I. Gnilitzkyi, V. Gruzdev, N. M. Bulgakova, L. Orazi, Appl.Phys.Lett **109**, 143101(2016).
- <sup>52</sup> M. V. Shugaev, I. Gnilitzkyi, N. M. Bulgakova, L. V. Zhigilei, Phys.Rev. B **96**, 205429 (2017).
- <sup>53</sup> M. L. Cohen, T. K. Bergstresser, Phys. Rev. **141**, 789 (1966).
- <sup>54</sup> J. E. Sipe, Ed. Ghahramani, Phys. Rev. B **48**, 11705 (1993).
- <sup>55</sup> W. H. Press, S. A. Tekuolsky, W. T. Vetterling, and B. P. Flannery, Numerical Recipes in FORTRAN (Cambridge University Press, Cambridge, 1993).
- <sup>56</sup> Lagomarsino, S., Sciortino, S., Obreshkov, B., Apostolova, T., Corsi, C., Bellini, M., Berdermann, E. and Schmidt, C.J Phys. Rev. B **93**.8 (2016): 085128
- <sup>57</sup> T. Apostolova, B. Obreshkov, Opt. Quant. Electron. **50**, 408 (2018).
- <sup>58</sup> A. A. Ionin, S. I. Kudryashov, S. V. Makarov, P. N. Saltuganov, L. V. Seleznev, D. V. Sinitsyn, and A. R. Sharipov, JETP Lett. **90**, 107 (2009).